Bubble Size Measurement in High-Density Air-Water Mixture Flows with Wide Size Distributions Using Digital Holography

Conference Paper · October 2009

DOI: 10.1364/FIO.2009.FThB1

4 authors, including:

Lei Tian
Boston University
115 PUBLICATIONS **2,286** CITATIONS
SEE PROFILE

Nick Loomis
[x]
11 PUBLICATIONS **198** CITATIONS
SEE PROFILE

Quantitative measurement of size and three-dimensional position of fast-moving bubbles in air–water mixture flows using digital holography

Lei Tian,[1,*] Nick Loomis,[1,2] José A. Domínguez-Caballero,[1] and George Barbastathis[1,3]

[1]Department of Mechanical Engineering, Massachusetts Institute of Technology, 77 Massachusetts Avenue, Cambridge, Massachusetts 02139, USA

[2]Applied Ocean Physics and Engineering Department, Woods Hole Oceanographic Institute, Woods Hole, Massachusetts 02543, USA

[3]Singapore-MIT Alliance for Research and Technology (SMART) Centre, Singapore 117543, Singapore

*Corresponding author: lei_tian@mit.edu

Received 4 November 2009; revised 18 February 2010; accepted 22 February 2010; posted 23 February 2010 (Doc. ID 119538); published 11 March 2010

We present a digital in-line holographic imaging system for measuring the size and three-dimensional position of fast-moving bubbles in air–water mixture flows. The captured holograms are numerically processed by performing a two-dimensional projection followed by local depth estimation to quickly and efficiently obtain the size and position information of multiple bubbles simultaneously. Statistical analysis on measured bubble size distributions shows that they follow lognormal or gamma distributions. © 2010 Optical Society of America

OCIS codes: 090.1995, 280.2490, 100.4995, 100.6890.

1. Introduction

Bubble sizing, counting, and locating problems occur in a wide variety of application areas, such as meteorology, fuel injection and combustion, chemical reactors, pollution, and cavitation. Many efforts have been devoted to their investigation by experimental methods and modeling approaches. Nevertheless, due to the complex fluid dynamics of turbulent three-dimensional (3D) two-phase flows, the physics of bubble formation, propagation, and annihilation is not well understood. Numerous imaging techniques have been developed for imaging bubbles in air–water mixture flows in the past decades. They can be summarized into three main categories: single-point measurement techniques, such as phase-Doppler imaging [1], planar imaging techniques, such as particle imaging velocimetry (PIV) [2], and 3D imaging techniques. Because of the 3D nature of two-phase flows, 3D imaging is preferable. Existing 3D imaging techniques, such as neutron radiography [3], scanning particle imaging [4], and defocusing digital particle imaging velocimetry [5] typically trade system complexity for spatial and temporal resolution.

Holography is well known for being able to record and reconstruct, in a single shot, information about

0003-6935/10/091549-06$15.00/0

an entire 3D volume of interest. Moreover, digital holography (DH) and digital holographic image processing [6] have become possible due to advances in megapixel electronic sensors, such as CCD and CMOS, with high space-bandwidth products. DH, compared to conventional holography, does not have the cumbersome requirement of film positioning, handling, and processing, and has the additional advantage that the information is readily available in digital form for postprocessing. DH has been increasingly used in a broad spectrum of applications, such as holographic PIV [7–9], plankton imaging [10,11], and holographic microscopy [12].

In this paper, we present a DH system for imaging fast-moving bubbles in air–water mixture flows. The system is designed to be compact, noninvasive, computationally efficient, and capable of analyzing large sample volumes. In Section 2, the experimental setup of our system is described. To decode the large amount of 3D information captured by a digital hologram, it is crucial to develop an automated data analysis algorithm. This algorithm is described in Section 3. In Section 4, experimental results are shown, followed by statistical analysis of the measured bubble size distribution. Some limitations of the present system and future improvement are discussed in Section 5.

2. Experimental System

An in-line digital holographic system is used to record two-phase flows. This has the benefit of being robust for field installations while maintaining simplicity in its components. The laboratory setup to create two-phase flows and holographically record bubbles in the flow is shown in Fig. 1. A DC motor drives a small propeller in a water tank to generate air bubbles. The dimensions of the tank are 100 mm × 100 mm × 70 mm and the central area is illuminated by a beam with a 36 mm diameter. The illumination is produced by a diode laser with wavelength of 658 nm. A programmable interface controller (PIC) microcontroller is used for generating a 5 μs pulse from the diode laser to effectively eliminate motion blur. The input beam is expanded by a spatial filter, and is collimated by a planoconvex lens. After propagating through the sample volume, the resultant hologram is recorded by a large space-bandwidth product CCD sensor. The sensor is a Kodak KAF16801E CCD with 4096 × 4096 pixels and 9 μm pixel pitch, resulting in a lateral resolution of 9 μm and depth of focus (DOF) of 300 μm on average for this particular geometry. The large detector size allows both a large cross-sectional sampling area and an extended working distance, within which both the lateral resolution and the DOF remain constant. All holograms are recorded when the bubble generation process is in equilibrium.

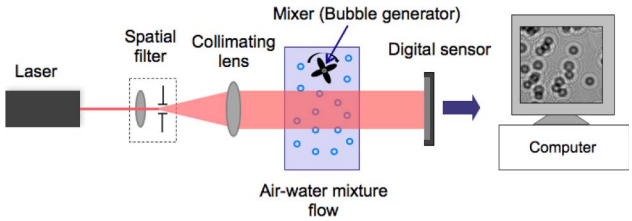

Fig. 1. (Color online) In-line digital holography experimental setup.

Assuming that the bubble density is not high enough to corrupt the collimated beam, the same beam serves both to illuminate the bubbles and as a reference beam. The hologram is the result of the interference between the undisturbed beam and light scattered by the bubbles. Figure 2 shows a 1024 × 1024 pixel portion of a sample hologram recorded by this system. The interference pattern from a single bubble is seen as a series of concentric rings in the hologram.

3. Automated Data Analysis

The DH recorded by the sensor encodes a vast amount of information about the bubbles contained in the sampled volume. Recovering details about the size and position follows a multistep process, similar to the methods proposed for extracting other types of information from holograms [11,13–15]. The volume is first reconstructed and a focus metric is applied to locate the objects. Once bubbles are found, the size and position are determined using image processing methods.

In the first stage, the hologram is reconstructed using the Fresnel approach to digitally backpropagate the field to multiple planes in the volume of interest [11]. At each step, the Fourier transform of the hologram is multiplied by the Fresnel transfer function at a given distance to find the spectral components at this distance from the sensor plane. Then, an inverse Fourier transform is applied to reconstruct the object field in the spatial domain from

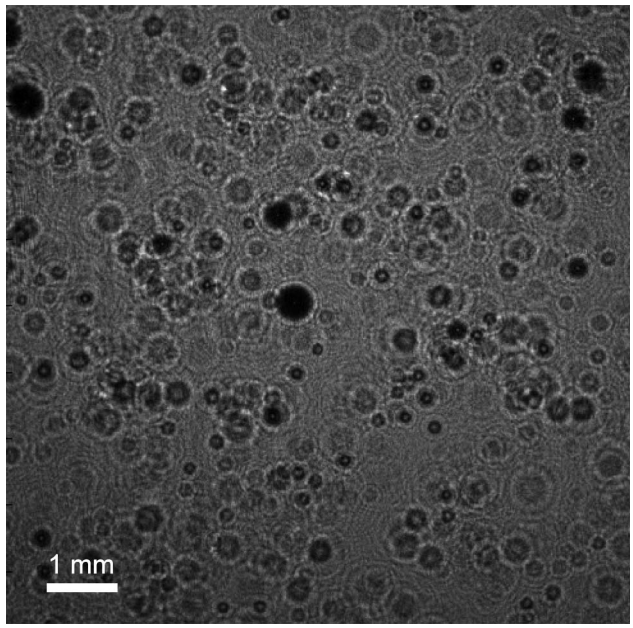

Fig. 2. A 1024 × 1024 pixel portion of a sample hologram of bubbles in an air–water mixture flow.

the computed spectra. The reconstructed field $R(x,y;z)$ is given by

$$R(x,y;z) = \mathcal{F}^{-1}\{\mathcal{F}\{I(x,y)\}(u,v) \cdot \mathcal{H}(u,v;z)\}, \quad (1)$$

where $I(x,y)$ is the hologram, $\mathcal{F}\{\bullet\}$ denotes the Fourier transform and $\mathcal{F}^{-1}\{\bullet\}$ the inverse, x and y are the lateral coordinates, z is the axial distance, and u and v are the transverse spatial frequencies. $\mathcal{H}(u,v;z)$ is the Fresnel approximated transfer function given by

$$\mathcal{H}(u,v;z) = \exp\{i\pi\lambda z(u^2+v^2)\}. \quad (2)$$

By changing the axial distance variable z in the Fresnel transfer function, it is possible to digitally reconstruct any plane within the volume of interest.

The next step is to extract information from the reconstruction. In limited cases where objects of interest have a highly constrained set of parameters, it may be possible to extract information about the objects directly from the hologram [11,16]. However, most real-world objects are not so fortuitously constrained or the pertinent information may not be available directly. This necessitates reconstructing the volume, often with image processing applied to every reconstruction plane, requiring significant computational and memory resources [7,15,17,18]. If *a priori* information is known about the final objective, only limited detail about each reconstruction is necessary to retain. This can result in much more efficient methods, such as presented here, where the object detection and segmentation is applied to a single two-dimensional (2D) plane that contains the salient details about the objects of interest. This algorithm is designed for analyzing two-phase flows with moderate bubble density, but the general routine may also be applicable to other cases, such as holographic PIV and plankton imaging.

In the first step, successive planes are reconstructed and the minimum intensity value at each pixel is recorded. This produces a 2D projection of the minimum intensity. At the same time, the axial position of where the minimum intensity occurred is recorded, creating a corresponding depth map. The minimum intensity is used here as a focus metric, which detects edges of the bubbles. Figure 3 shows an example of the reconstructed intensity for a bubble 17.5 mm from the hologram; the edge pixels a, b, and c reach minimum intensities at the same depth, while the interior pixel, d, has a different minimum due to the formation of caustics. This minimum intensity focus metric is applied to the hologram shown in Fig. 2. The resulting minimum intensity projection and corresponding depth map are shown in Figs. 4(a) and 4(b), respectively.

The second step of the algorithm uses the intensity information to locate bubbles. The minimum intensity projection is thresholded to create a map of bubble edges. Morphological operators are used to reconnect nearby regions through a dilation and an erosion process. An example is depicted in Fig. 4(c), where the thresholding creates a binary edge mask. This edge mask can then be used with the depth map to estimate depths of objects, similar to [19], which attempts to use a rough depth map with large objects. The benefit of this technique is that it provides a depth estimate for every object in the hologram.

Two-phase flows face an additional challenge: because bubbles are distributed throughout the volume, there is a chance of overlapping edges in the intensity projection and depth maps. This appears as two or more distinct depths within a segmented edge map. A Gaussian mixture model (GMM) [20] is used to determine the most likely number and depths of the bubbles represented in each edge segment. GMMs with varying number of mixture components are fit to the depth distribution for each edge segment, and the minimum Rissanen value [21] is used to select the most likely model. The mean of each mixture component gives the bubble depth. Edges corresponding to single bubbles also benefit from this approach, as it statistically removes some of the measurement noise, which is appropriate given *a priori* knowledge that the bubble edge should appear at a single depth plane. A refined depth map, such as shown in Fig. 4(d), is built from the GMM results. Figure 5 shows an example of how the

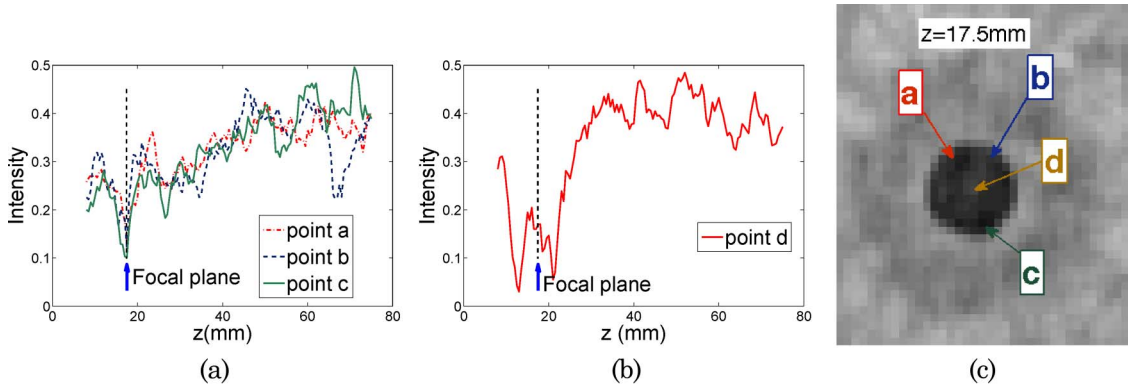

Fig. 3. (Color online) Demonstration of the edge minimum intensity focus metric. (a) intensity "column" corresponding to edge pixels a, b, and c as a function of distance z from the camera plane. The intensity is minimum at the focal plane. (b) In the intensity "column" for interior pixel d, the intensity is *not* minimum at the focal plane. (c) Intensity projection near a bubble that was located at $z = 17.5$ mm.

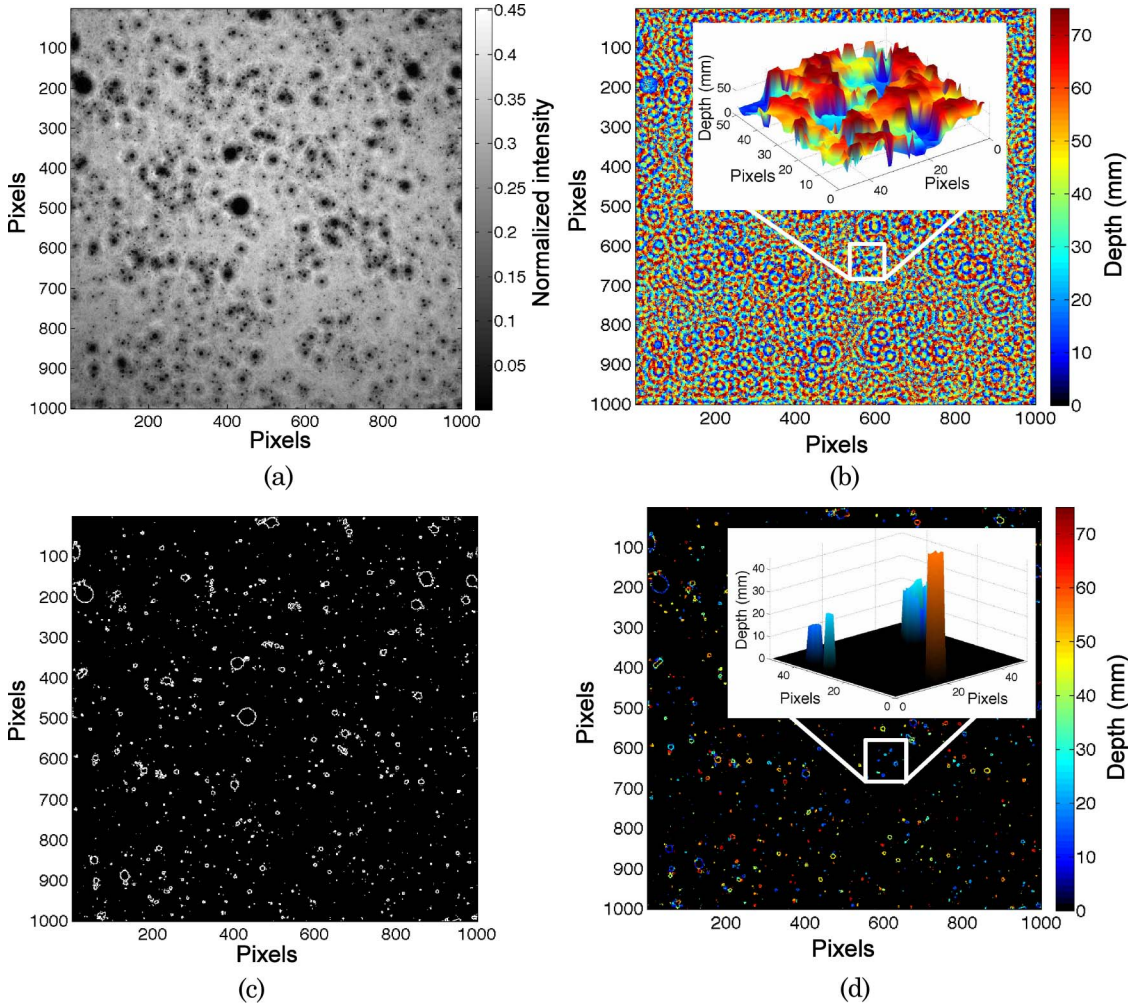

Fig. 4. (Color online) Diagram of key steps of the proposed DH data analysis algorithm. (a) Intensity projection that contains all the in-focus pixels. (b) The original depth map that records the axial position of every pixel. (c) Extracted edges of the thresholded intensity projection. (d) Refined depth map records only the axial value of in-focus bubble edges.

GMM separates six overlapping bubbles that share a common edge segment.

Finally, size and 3D position information for each bubble is obtained from the corresponding segments of the refined depth map. Bubble sizes are measured from the equivalent diameters computed from the areas enclosed by each edge.

4. Results

The proposed algorithm can be run in near real time. The most time-consuming step in the proposed algorithm is in generating the minimum intensity projection and corresponding depth map. However, the FFT-based reconstruction is easily implemented on a graphics processing unit (GPU) using NVidia CUDA [22] for fast computation. Using a midrange NVidia GeForce 9800 GT GPU, 135 reconstruction planes of a 1024 × 1024 pixel hologram can be reconstructed in 0.85 s, 150 times faster than a CPU-only reconstruction. The morphological operations and GMMs are computed on the resulting minimum intensity projection in MATLAB. The total computation time is less than 4.3 s per hologram.

An example result from a single hologram is shown in Fig. 6. A 3D visualization of the positions and sizes of the bubbles recorded in this hologram is shown in Fig. 6(a). Bubble sizes are scaled for visibility, with color indicating bubble diameters. Figure 6(b) shows

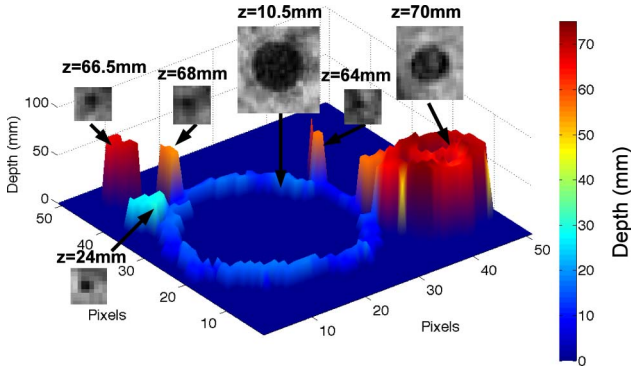

Fig. 5. (Color online) Depth map resulting from six bubbles whose intensity projections overlap. After applying a GMM, they are successfully separated and their individual axial positions are determined. In-focus bubble images are shown in the insets.

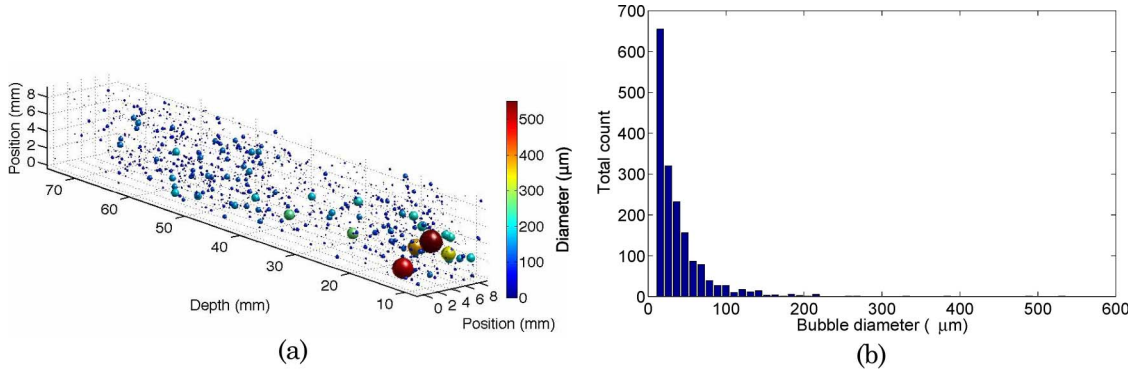

Fig. 6. (Color online) Data processing result from a 1024 × 1024 pixel hologram. (a) 3D visualization of data processing results from a single hologram (diameters not to scale). (b) Bubble size distribution.

the bubble size distribution histogram. The first bin corresponds to the CCD's pixel size and accumulates all detectable bubbles smaller than 9 μm. In this hologram, 1699 bubbles are detected with diameters ranging from less than 9 μm (the detector pixel size) to 600 μm. Fluid mechanics literature suggests that the air bubble generation process employed should produce bubbles with size statistics following lognormal or gamma distributions [23,24]. The probability density function of the lognormal distribution is

$$f(d;\mu,\sigma) = \frac{1}{d\sigma\sqrt{2\pi}} e^{-\frac{(\ln d-\mu)^2}{2\sigma^2}}, \tag{3}$$

where d is the diameter of the bubble, μ is the mean of the bubble diameter's natural logarithm, and σ is the standard deviation of the bubble diameter's natural logarithm. The gamma distribution probability density function is

$$f(d;a,b) = d^{a-1}\frac{e^{-d/b}}{b^a\Gamma(a)}, \tag{4}$$

where $\Gamma(\bullet)$ is the gamma function, a is the shape parameter, and b is the scale parameter. The bubble size data are fit to these distributions. The probability density fit for the bubble size data from one hologram is shown in Fig. 7. Both lognormal and gamma distributions are reasonable fits to the size distributions, passing a χ^2 goodness-of-fit test [25] at the 5% significance level.

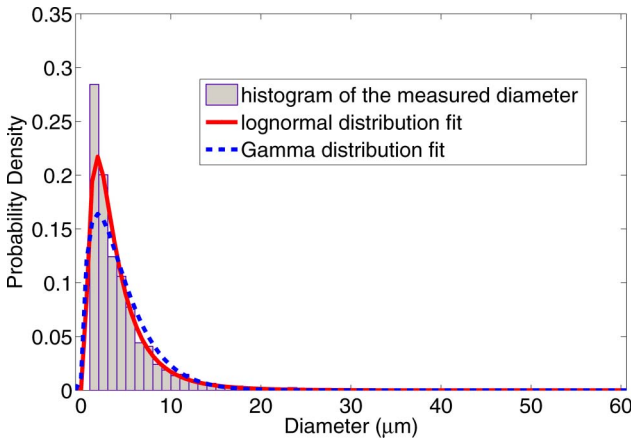

Fig. 7. (Color online) Histogram of bubble sizes and probability distribution fits.

5. Conclusion

An in-line digital holographic imaging system for measuring size and 3D position of fast-moving bubbles in air–water mixture flows is presented. An automated data analysis algorithm has been developed. The proposed algorithm uses the 2D projection scheme to generate a depth map that records the axial position of bubbles. A GMM is applied to separate overlapping information on the projected intensity map. This algorithm has the advantage that size and position information of multiple objects is extracted simultaneously with only 2D data computations so that axially overlapping bubbles can be resolved. This algorithm is designed for analyzing two-phase flows with moderate bubble density, but the general routine may also be applicable to other cases, such as holographic PIV and plankton imaging. The limitation of this algorithm is that it cannot deal with a very high density of bubbles, in which a fully 3D algorithm would be required. The statistical analysis on the measured bubble size distribution shows good agreement with a lognormal or a gamma distribution, as suggested in the fluid mechanics literature. This paper demonstrates that DH is a promising quantitative measurement technique in two-phase flow research.

This work was supported by the Chevron-MIT Energy Initiative Deepwater Sponsored Research Project University Partnership Program, Technology Development for Deepwater Research (Deepstar), and the Center for Environmental Sensing and Modeling (CENSAM) under the Singapore-MIT Alliance for Research and Technology (SMART) Centre.

References

1. A. Naqwi, F. Durst, and G. Kraft, "Sizing of submicrometer particles using a phase-Doppler system," Appl. Opt. **30**, 4903–4913 (1991).
2. R. J. Adrian, "Twenty years of particle image velocimetry," Exp. Fluids **39**, 159–169 (2005).

3. K. Mishima and T. Hibiki, "Development of high-frame-rate neutron radiography and quantitative measurement method for multiphase flow research," Nucl. Eng. Des. **184**, 183–201 (1998).
4. C. Brücker, "3D scanning PIV applied to an air flow in a motored engine using digital high-speed video," Meas. Sci. Technol. **8**, 1480–1492 (1997).
5. F. Pereira, M. Gharib, D. Dabiri, and D. Modarress, "Defocusing digital particle image velocimetry: a 3-component 3-dimensional DPIV measurement technique. Application to bubbly flows," Exp. Fluids **29**, S78–S84 (2000).
6. U. Schnars and W. Jueptner, *Digital Holography: Digital Hologram Recording, Numerical Reconstruction, and Related Techniques* (Springer, 2005).
7. G. Pan and H. Meng, "Digital holography of particle fields: reconstruction by use of complex amplitude," Appl. Opt. **42**, 827–833 (2003).
8. J. A. Dominguez-Caballero and G. Barbastathis, "Stability of the digital holographic inverse problem as a function of particle density," in *Digital Holography and Three-Dimensional Imaging* (Optical Society of America, 2008), paper PDPJMA6.
9. Y. Pu and H. Meng, "Four-dimensional dynamic flow measurement by holographic particle image velocimetry," Appl. Opt. **44**, 7697–7708 (2005).
10. J. A. Dominguez-Caballero, N. Loomis, W. Li, Q. Hu, J. Milgram, G. Barbastathis, and C. Davis, "Advances in plankton imaging using digital holography," in *Computational Optical Sensing and Imaging* (Optical Society of America, 2007), paper DMB5.
11. J. H. Milgram and W. Li, "Computational reconstruction of images from holograms," Appl. Opt. **41**, 853–864 (2002).
12. D. Carl, B. Kemper, G. Wernicke, and G. Bally, "Parameter-optimized digital holographic microscope for high-resolution living-cell analysis," Appl. Opt. **43**, 6536–6544 (2004).
13. J. A. Dominguez-Caballero, "Digital holographic imaging of aquatic species," Master's thesis (Massachusetts Institute of Technology, 2006).
14. J. P. Fugal, T. J. Schulz, and R. A. Shaw, "Practical methods for automated reconstruction and characterization of particles in digital in-line holograms," Meas. Sci. Technol. **20**, 075501 (2009).
15. S. Satake, H. Kanamori, T. Kunugi, K. Sato, T. Ito, and K. Yamamoto, "Parallel computing of a digital hologram and particle searching for microdigital-holographic particle-tracking velocimetry," Appl. Opt. **46**, 538–543 (2007).
16. F. C. Cheong, B. Sun, R. Dreyfus, J. Amato-Grill, K. Xiao, L. Dixon, and D. G. Grier, "Flow visualization and flow cytometry with holographic video microscopy," Opt. Express **17**, 13071–13079 (2009).
17. F. Dubois, C. Schockaert, N. Callens, and C. Yourassowsky, "Focus plane detection criteria in digital holography microscopy by amplitude analysis," Opt. Express **14**, 5895–5908 (2006).
18. W. Li, N. Loomis, Q. Hu, and C. S. Davis, "Focus detection from digital in-line holograms based on spectral l_1 norms," J. Opt. Soc. Am. A **24**, 3054–3062 (2007).
19. M. L. Tachiki, M. Itoh, and T. Yatagai, "Simultaneous depth determination of multiple objects by focus analysis in digital holography," Appl. Opt. **47**, D144–D153 (2008).
20. D. Reynolds and R. Rose, "Robust text-independent speaker identification using Gaussian mixture speaker models," IEEE Trans. Speech Audio Process. **3**, 72–83 (1995).
21. J. Rissanen, "Stochastic complexity and modeling," Ann. Stat. **14**, 1080–1100 (1986).
22. NVidia, http://www.nvidia.com/object/cuda_home_new.html.
23. J. Varley, "Submerged gas-liquid jets—bubble-size prediction," Chem. Eng. Sci. **50**, 901–905 (1995).
24. H. Chanson, "Air bubble entrainment in open channels: flow structure and bubble size distributions," Int. J. Multiphase Flow **23**, 193–203 (1997).
25. R. B. D'Agostino and M. A. Stephens, *Goodness-of-Fit Techniques*, Vol. 68 of Statistics, Textbooks and Monographs (Marcel-Dekker, 1986).